PHILOSOPHICAL MAGAZINE A, 2002, VOL. 82, NO. 14, 2737–2754

Taylor & Francis
Taylor & Francis Group

Transmission electron microscopy analysis of planar faults on (001) planes in $MoSi_2$ single crystals

SUSANNE GUDER†, MARTIN BARTSCH and ULRICH MESSERSCHMIDT‡

Max Planck Institute of Microstructure Physics, Halle/Saale, D-06120, Germany

[*Received 9 May 2001 and accepted in revised form 28 April 2002*]

ABSTRACT

Planar faults on (001) planes were formed during *in-situ* annealing and straining experiments on $MoSi_2$ single crystals in a high-voltage electron microscope. As-received and pre-deformed crystals grown by either the float-zone or the Czochralski technique were exposed to temperatures between 400 and 1200°C. The faults are only formed if dislocations with $\frac{1}{2}\langle 111\rangle$ Burgers vectors are present. The faults and the bordering partial dislocations were characterized by a transmission electron microscopy contrast analysis. The two partial dislocations bordering a fault have different types of Burgers vector. It is suggested that the faults result from a dissociation reaction according to $\frac{1}{2}[111] = \frac{1}{2}[110] + \frac{1}{2}[001]$, leading to intrinsic stacking faults on (001) planes. Probably, similar microstructural mechanisms control both the formation of the faults and the flow stress anomaly of the $\langle 111\rangle\{110\}$ slip system in $MoSi_2$.

§1. INTRODUCTION

Several recent publications describe planar faults on (001) planes in $MoSi_2$ (Umakoshi *et al.* 1989, 1990, Kimura *et al.* 1990, Hirano *et al.* 1991, Mitchell and Maloy 1993, Maloy *et al.* 1995, Kad *et al.* 1995, Ito *et al.* 1996, 1997, Evans *et al.* 1997). They were first interpreted incorrectly as stacking faults on {110} planes as a consequence of a suggested stress-induced phase transformation from the $C11_b$ to the C40 structure (Umakoshi *et al.* 1989, 1990, Kimura *et al.* 1990, Hirano *et al.* 1991). The phase instability was thought to be responsible for the formation of partial dislocations with $\frac{1}{4}\langle 111\rangle$ Burgers vectors, which form stacking faults by moving on their {110} slip planes. However, the C40 structure is considered a hexagonal high-temperature phase in the Mo–Si system formed at temperatures above 1900°C. It has not been observed in stoichiometric $MoSi_2$ (Boettinger *et al.* 1992), which is regarded as stable up to its melting point (Frankwicz *et al.* 1993). The contradictions were solved by a reinterpretation of the experimental observations by Kad *et al.* (1995). Accordingly, the planar faults observed by Umakoshi *et al.* (1989) lie on (001) planes. Still, the results about the character and the density of the (001) faults in $MoSi_2$ single crystals differ considerably (Kad *et al.* 1995, Ito *et al.* 1997, Guder *et al.* 1999, Guder 2000). Taking into account the results on faults observed after deformation (Mitchell and Maloy 1993, Maloy *et al.* 1995), actually two processes

† Present address: Department of Materials in Mechanical Engineering, Technical University Munich, D-85747 Garching, Germany.

‡ Author for correspondence. Email: um@mpi-halle.de.

Philosophical Magazine A ISSN 0141–8610 print/ISSN 1460-6992 online
http://www.tandf.co.uk/journals
DOI: 10.1080/01418610210155753

are proposed for the formation of planar faults on (001) planes in $MoSi_2$. One consists of a dissociation of dislocations with the $\frac{1}{2}\langle 331\rangle$ Burgers vector at 1000°C (Maloy *et al.* 1995) or with the $\frac{1}{2}\langle 111\rangle$ Burgers vectors at 1400°C (Mitchell and Maloy 1993), given by

$$\tfrac{1}{2}\langle 331\rangle \rightarrow \tfrac{1}{6}\langle 331\rangle + \tfrac{1}{6}\langle 331\rangle + \tfrac{1}{2}\langle 010\rangle + \tfrac{1}{6}\langle 301\rangle, \quad (1)$$

$$\tfrac{1}{2}\langle 111\rangle \rightarrow \tfrac{1}{6}\langle 301\rangle + \tfrac{1}{2}\langle 010\rangle + \tfrac{1}{3}\langle 001\rangle, \quad (2)$$

$$\tfrac{1}{2}\langle 111\rangle \rightarrow \tfrac{1}{3}\langle 001\rangle + \tfrac{1}{6}\langle 331\rangle, \quad (3)$$

owing to climb processes during compressive deformation at high temperatures. These diffusion-controlled climb dissociations lead to complex stacking faults and antiphase boundaries on (001) planes respectively. Further publications confirming these results are not known. As a second process, the formation of grown-in condensation faults on (001) planes is considered (Kad *et al.* 1995, Ito *et al.* 1996, 1997) owing to a loss of Si during the growth of $MoSi_2$ single crystals at temperatures up to 1600°C (Kad *et al.* 1995, Ito *et al.* 1997). These faults are bordered by Frank-type dislocations having a Burgers vector parallel to [001].

The present authors observed planar faults on (001) planes first during *in-situ* straining experiments on $MoSi_2$ single crystals in a high-voltage electron microscope at high temperatures (Guder *et al.* 1999). The observations did not agree with the previous interpretations. Therefore, additional *in-situ* straining and *in-situ* annealing studies were performed in the high-voltage electron microscope with the aim of characterizing these faults by a systematic transmission electron microscopy (TEM) contrast analysis in the high-voltage electron microscope and to find the mechanism of their formation.

§ 2. Theory

Methods to characterize planar translation interfaces by diffraction contrast in the transmission electron microscope have been given by Art *et al.* (1963), Gevers *et al.* (1963) and Amelinckx *et al.* (1978). An interface is described either by its displacement vector $\mathbf{R}$ within the interface or by the fault vector $\mathbf{R}_F$. While $\mathbf{R}$ characterizes the displacement of the neighbouring crystal parts below and above the interface against each other, $\mathbf{R}_F$ describes the displacement in the stacking sequence perpendicular to the interface. As in general $\mathbf{R}$ and $\mathbf{R}_F$ differ by a translation vector of the lattice, both are equivalent with respect to the diffraction contrast analysis. In ordered structures, additionally antiphase boundaries are possible. Then $\mathbf{R}_F$ is a lattice vector for the disordered structure but not for the ordered one.

For the ordered tetragonal structure of $MoSi_2$, three faults on (001) planes may exist with the respective fault vectors $\mathbf{R}_F$ of $\frac{1}{6}\langle 001\rangle$, $\frac{1}{3}\langle 001\rangle$ and $\frac{1}{2}\langle 001\rangle$, as shown in figure 1. While $\mathbf{R}_F$ vectors of $\frac{1}{6}\langle 001\rangle$ and $\frac{1}{2}\langle 001\rangle$ cause simple stacking faults, $\mathbf{R}_F = \frac{1}{3}\langle 001\rangle$ corresponds to an antiphase boundary. $\mathbf{R}_F = \frac{1}{2}\langle 001\rangle$ can be expressed by a combination of a displacement vector in the (001) interface and a translation vector of the $C11_b$ structure, that is $\frac{1}{2}\langle 110\rangle$ and $\frac{1}{2}\langle 111\rangle$ respectively. Equivalent expressions do not exist for $\mathbf{R}_F = \frac{1}{6}\langle 00\bar{1}\rangle$ and $\frac{1}{3}\langle 00\bar{1}\rangle$. Planar interfaces with $\mathbf{R}_F$ vectors of $\frac{1}{6}\langle 001\rangle$ and $\frac{1}{3}\langle 001\rangle$ cannot be generated by a glide displacement in the (001) interface. They arise either from climb-assisted dislocation dissociations according to equations (2) and (3) or from diffusion processes in the Si(001) layers, only. In the latter case, the disorder in the stacking sequence of the (001) planes corresponds to a stacking-fault-like interface if a single Si(001) layer is removed and

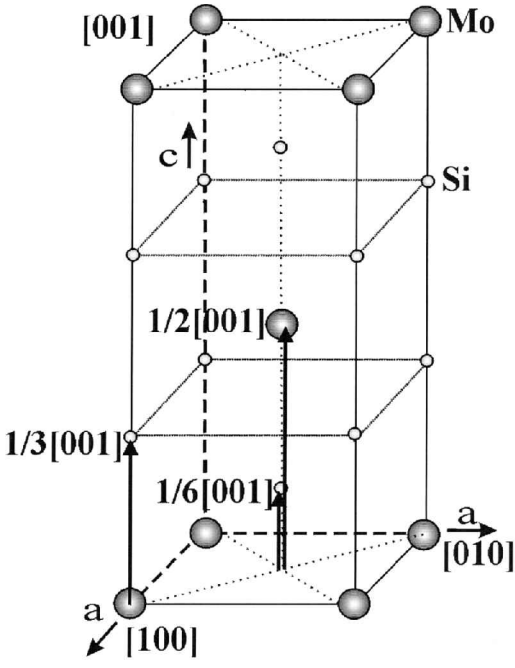

Figure 1. Fault vectors $\mathbf{R}_F$ for (001) interfaces in $MoSi_2$.

to an antiphase boundary-like interface if two adjacent Si(001) layers are removed. Both interfaces are bordered by a partial dislocation loop of Frank type with a Burgers vector perpendicular to the loop plane equal to the respective fault vector $\mathbf{R}_F$. In $MoSi_2$, a loss of Si during crystal growth rather than a condensation of Si lattice vacancies (Kad *et al*. 1995, Ito *et al*. 1997) is assumed to cause a loss of one or two adjacent Si(001) layers and is described by $\mathbf{R}_F = \mathbf{b} = \frac{1}{6}\langle 001\rangle$ or $\frac{1}{3}\langle 001\rangle$ respectively.

For planar faults on (001) planes in $MoSi_2$ the direction of the fault vector $\mathbf{R}_F$ is easily determined by an extinction of the fringe contrast for $\mathbf{g}\cdot\mathbf{R}_F = 0$ using imaging vectors $\mathbf{g}$ perpendicular to $\mathbf{R}_F$. The absolute value of $\mathbf{R}_F$ is determined by an extinction of fringe contrast for $\mathbf{g}\cdot\mathbf{R}_F = n$ with $n = 1, 2, \ldots$, that is with $\mathbf{g}$ not perpendicular to $\mathbf{R}_F$. For interfaces on (001) planes, the relation $\mathbf{g}\cdot\mathbf{R}_F = n$ with $\mathbf{g} = [HKL]$ and $\mathbf{R}_F = (1/m)\langle 001\rangle$ can be simplified to

$$\frac{L}{m} = n,\ n = 1, 2, 3, \ldots. \tag{4}$$

The structure factor effect leads to the presence of reflections of planes (*hkl*) with an even sum of $h + k + l$ in the $C11_b$ structure. Fundamental reflections additionally require that the index l is a multiple of 3.

§ 3. Experimental procedure

As mentioned above, planar faults on (001) planes were first observed by the present authors during *in-situ* straining experiments on $MoSi_2$ single crystals along [201] in a high-voltage electron microscope at about 1000°C (Guder *et al*. 1999). In order to find the mechanism of the fault formation, further *in-situ* straining and *in-*

situ annealing experiments were performed in the high-voltage electron microscope. The specimens were prepared from as-received float-zone (FZ) and Czochralski (CZ)-grown single crystals and from those pre-deformed in macroscopic compression tests at different orientations and temperatures. The compression tests were performed on crystal bars of dimensions about $5\,\text{mm} \times 2\,\text{mm} \times 1\,\text{mm}$ or $10\,\text{mm} \times 2\,\text{mm} \times 1\,\text{mm}$ at a strain rate of $10^{-5}\,\text{s}^{-1}$. The preparation routine of the microtensile specimens for *in-situ* straining experiments has been explained elsewhere (Guder *et al.* 1999). Mostly, pre-deformed material was used for these experiments with the tensile axis parallel to the compression axis of the pre-deformation. Foils for *in-situ* annealing experiments were prepared like conventional TEM foils, that is by cutting slices of about 300 µm thickness by spark erosion followed by grinding and polishing down to a thickness of about 100 µm, dimpling the centre to a residual thickness of about 20–30 µm and finally ion milling with Ar ions to perforation.

The *in-situ* deformation experiments were performed in a double-tilting high-temperature straining stage described by Messerschmidt and Bartsch (1994) inside a high-voltage electron microscope operated at 1000 kV at temperatures between about 400 and 1000°C. The load acting on the specimen is measured by semiconducting strain gauges and is usually increased in small load increments. The microstructure and its changes were recorded either on photographic film or on video tape. The *in-situ* annealing experiments were performed in a conventional double-tilting

Table 1. History of deformation and heat treatments for all specimens investigated.

Specimen	Growth method	Macroscopic deformation		*In-situ* deformation and annealing		Faults on (001)
		LA	T_C(°C)	LA	$T_{in\,situ}$(°C)	
A	FZ	—	—	—	—	No
B	FZ	—	—	—	—	A single fault
C	CZ	—	—	—	—	No
D	FZ	—	—	—	650	No
E	CZ	—	—	[110]	650, 950, 1050, 1250	No
F	CZ	—	—	[110]	650	No
G	FZ	—	—	[201]	800	Yes
H	FZ	[201]	300, 400, 600	—	—	No
I	FZ	[201]	350	—	—	No
J	FZ	[201]	750	—	—	No
K	FZ	[201]	500, 850, 500	—	—	No
L	FZ	[201]	1200	—	—	No
M	FZ	[302]	990, 1200	—	—	No
N	FZ	[18 0 1]	1200	—	—	No
O	CZ	[110]	600, 790, 1200	—	—	No
P	CZ	[110]	1200	—	—	No
Q	FZ	[302]	990, 1200	—	550	Yes
R	FZ	[201]	500, 850, 500	—	630	Yes
S	FZ	[201]	300, 400, 600	—	670	Yes
T	FZ	[18 0 1]	1200	—	790	Yes
U	FZ	[201]	400	[201]	440	Yes
V	FZ	[201]	300	[201]	450	Yes
W	FZ	[201]	1200	[201]	1000	Yes
X	CZ	[110]	600, 790, 1200	—	650	No

heating stage inside the high-voltage electron microscope. Usually, the specimens were heated stepwise with increments of about 60 K. A constant specimen temperature was achieved after 10 min. The defects produced during the *in-situ* straining and annealing experiments were characterized in detail by a post-mortem TEM analysis at room temperature using a wide-angle goniometer capable of a specimen tilt of about $\pm 45°$ around two axes.

The history of the deformation and heat treatments of all specimens investigated is summarized in table 1. LA is the orientation of the loading axis; the LAs are the same in the macroscopic compression and the *in-situ* tensile experiments. Furthermore, the table lists the temperature T_C of the compression experiments and the maximum temperature $T_{in\,situ}$ of the *in-situ* experiments. In some cases a single compression bar or microtensile specimen was tested at different temperatures. Then, the temperatures are given in the order of testing. The choice of LA and especially of the foil normal of the TEM specimens was limited by the small thickness of the available platelets of the starting material. Therefore, all FZ crystals have a foil normal parallel to [010] and a LA of [201], [302] or [18 0 1] and all CZ crystals have a foil normal parallel to $[1\bar{1}0]$ and a LA of [110].

§4. Results

4.1. *Formation of planar faults on (001) planes*

The $MoSi_2$ single crystals investigated by electron microscopy and listed in table 1 can be divided into the following groups:

(i) as-received crystals (specimens A to C);
(ii) as-received and *in-situ* annealed or strained crystals (specimens D to G);
(iii) macroscopically deformed crystals (specimens H to P);
(iv) macroscopically deformed and *in-situ* annealed or strained crystals (specimens Q to X).

The preparation of microtensile specimens of crystals pre-deformed along [110] was not successful. Depending on the LA orientation of both macroscopically and *in-situ* strained crystals, the $\langle 111\rangle\{110\}$ slip system was activated in FZ crystals with a LA of [201], [302] or [18 0 1] and the $\langle 100\rangle\{101\}$ system in CZ crystals with a LA of [110]. While the starting FZ material was almost free of precipitates, CZ specimens typically contained Mo_5Si_3 platelets.

The results of all experiments with respect to the occurrence of planar faults are listed in the fourth column of table 1 and can be summarized in the following way. Planar faults on (001) planes were always observed after *in-situ* annealing or straining experiments on crystals either containing dislocations with $\frac{1}{2}\langle 111\rangle$ Burgers vectors due to a pre-deformation (specimens Q to W) or acquiring these dislocations during the *in-situ* straining experiments (specimen G) in the high-voltage electron microscope. The respective temperatures range from approximately 440 to 1000°C. In all cases, faults were only formed if dislocations with $\frac{1}{2}\langle 111\rangle$ Burgers vectors were present. Although *in-situ* experiments offer the possibility to observe microstructural changes such as dislocation motion or the formation of sufficiently large defects directly, in none of these experiments has the formation of the faults directly been observed since it occurred in an instantaneous way. Also, changes in the fault size after the sudden formation have never been observed during the further course of the experiments. In all other cases listed above, that is crystals containing $\frac{1}{2}\langle 111\rangle$ dis-

locations after macroscopic compression (specimens H to N) and in the absence of $\frac{1}{2}\langle 111\rangle$ dislocations (specimens A, C to F, O, P and X), the formation of faults has never been observed. The single fault observed in specimen B is an exception. Again the fault is located in the vicinity of dislocations. However, the foil thickness impeded a contrast analysis of both the fault and the dislocations.

Figure 2 presents the formation of planar faults in specimen **R** during an *in-situ* annealing experiment. Figure 2 (*a*) exhibits a specimen area with dislocations of $\frac{1}{2}[111]$ Burgers vectors on $(1\bar{1}0)$ planes generated during the pre-deformation. The dislocations are straight and aligned near the crystallographic [110], $[11\bar{1}]$ and $[33\bar{1}]$ directions. The specimen was continuously heated inside the high-voltage electron microscope to a final temperature of 630°C. At this temperature, faults on (001) planes suddenly formed on the dislocations, particularly on those in the [110] direction. The undissociated $\frac{1}{2}[111]$ dislocations are extinguished for the imaging vector $(\bar{1}01)$ in figure 2 (*b*). The post-mortem TEM analysis in figures 2 (*c*) and (*d*) confirms the existence of several planar faults on (001) planes and their bordering partial dislocations. They are imaged at the $[0\bar{3}\bar{1}]$ beam direction with the imaging vectors (200) and $(2\bar{1}3)$. We consider the new partials as imaged in strong residual contrast in figure 2 (*c*). A detailed contrast analysis of the partials is given in § 4.2. During the annealing experiment, small lobes decorating the dislocations disappeared (compare figure 2 (*a*) with figures 2 (*b*)–(*d*)). The lobes are artefacts of the ion-beam thinning and were characterized as circular defects by Boldt *et al.* (1997). Several annealing experiments (specimens Q to T) confirmed the generation of faults on (001) planes at temperatures between 550 and 670°C.

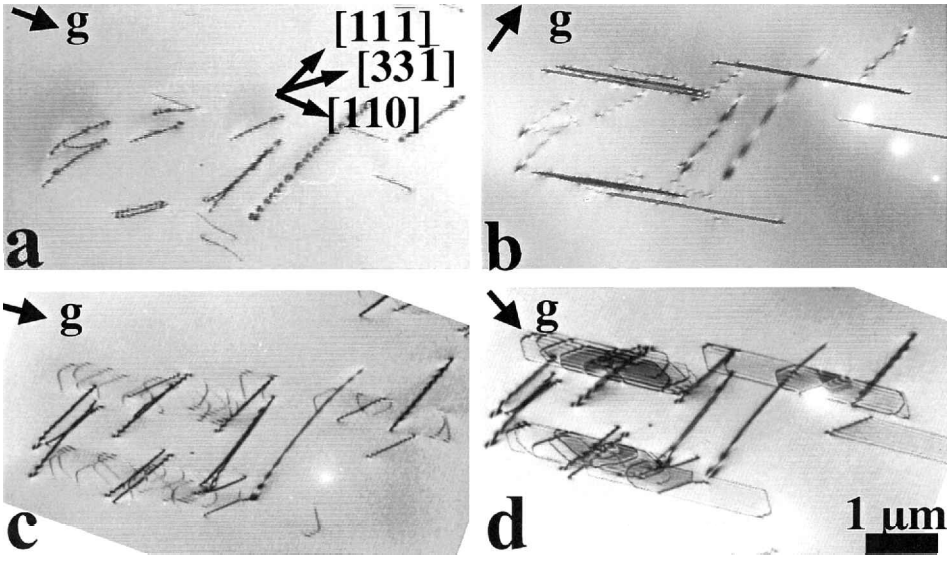

Figure 2. Formation of planar faults on (001) planes on dislocations with a $\frac{1}{2}[111]$ Burgers vector during an *in-situ* annealing experiment on an $MoSi_2$ single crystal (specimen R). (*a*) Microstructure with $\frac{1}{2}[111]$ dislocations after macroscopic compression; $\mathbf{g} = (200)$, beam direction (BD) of approximately [010]; the arrows show the projections of the respective directions on to the image plane. (*b*) Sudden formation of faults during *in-situ* annealing at about 630°C; $\mathbf{g} = (\bar{1}01)$ and BD of approximately [010]. (*c*), (*d*) Several faults along a single $\frac{1}{2}[111]$ dislocation: (*c*) $\mathbf{g} = (200)$; (*d*) $\mathbf{g} = (2\bar{1}3)$; post-mortem analysis at room temperature at a BD of approximately $[0\bar{3}\bar{1}]$.

The size and density of the faults depend on the type of *in-situ* experiment, as demonstrated in figures 3 (*a*) and (*b*). In specimen T of figure 3 (*a*), the faults formed spontaneously during heating to 790°C without an external load while specimen W in figure 3 (*b*) experienced an external load at 1000°C. In general, after *in-situ* annealing experiments (specimens D, Q to T and X), the partial dislocations bordering the faults are separated by a few micrometres. After *in-situ* straining experiments (specimens G and U to W), much larger separations of the partial dislocations are

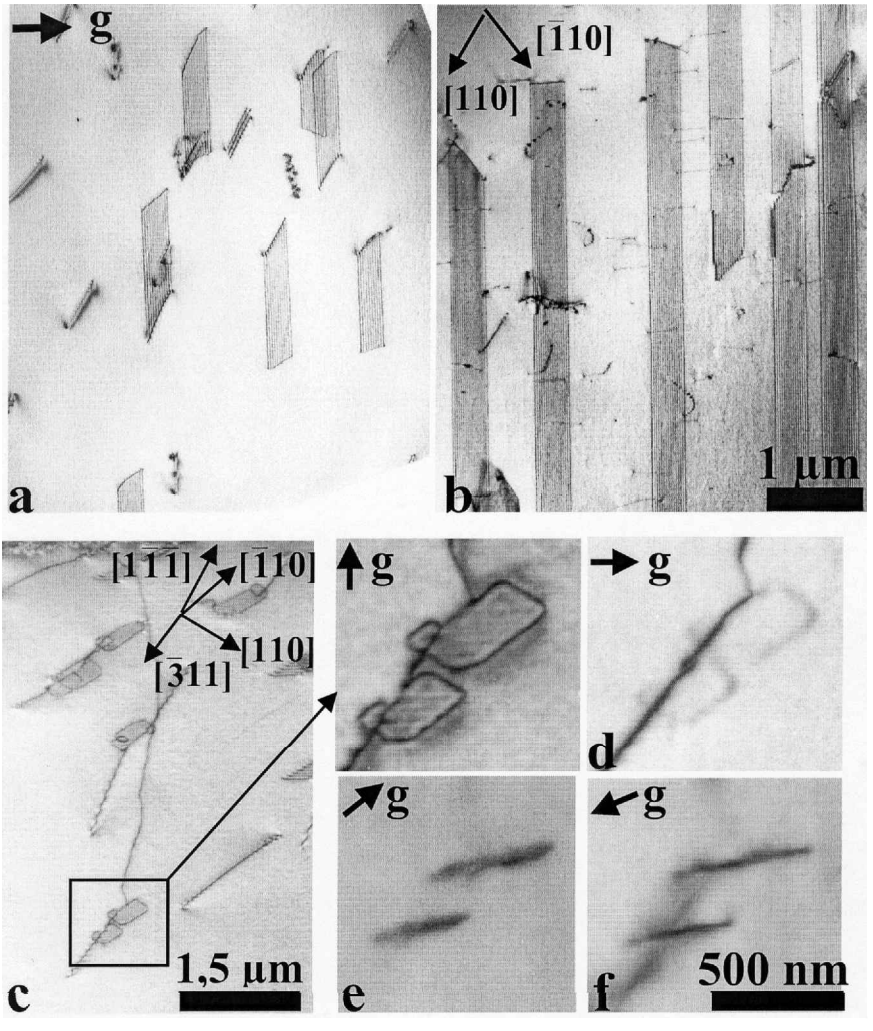

Figure 3. Dissociation of $\frac{1}{2}\langle 111\rangle$ dislocations during (*a*) *in-situ* annealing of specimen T at 790°C, and (*b*) *in-situ* straining of specimen W at 1000°C, both containing $\frac{1}{2}\langle 111\rangle$ dislocations with orientations near $\langle 110\rangle$: (*a*), (*b*) $\mathbf{g} = (013)$ and a BD of approximately $[03\bar{1}]$. (*c*)–(*f*) Dissociation of a dislocation having a $\frac{1}{2}[1\bar{1}1]$ Burgers vector and a $[\bar{3}31]$ line direction during *in-situ* annealing of specimen S at 670°C, where the indexed arrows mark the projections of the respective directions on to the image plane: (*c*) $\mathbf{g} = (0\bar{1}\bar{3})$ and a BD of approximately $[03\bar{1}]$; (*d*) $\mathbf{g} = (200)$ and a BD of approximately $[03\bar{1}]$; (*e*) $\mathbf{g} = (2\bar{1}\bar{3})$ and a BD of approximately [120]; (*f*) $\mathbf{g} = (\bar{1}01)$ and a BD of approximately [010]. After dissociation, the branches of the partial dislocation loop align along [110] and $[\bar{1}10]$.

observed from several micrometres up to even more than 10 μm in specimen W. Although the latter experiment took several hours, the wide faults formed at the beginning of the straining did not change their size during the ongoing experiment.

The formation of the faults is also influenced by the orientation of the affected $\frac{1}{2}\langle 111\rangle$ dislocations as demonstrated by comparing the fault sizes in figures 3 (*a*) and (*b*) with those in figures 3 (*c*)–(*f*). In all crystals investigated, $\frac{1}{2}\langle 111\rangle$ dislocations with an orientation near $\langle 110\rangle$ dissociated along their whole length within the TEM foil and exhibit a width of a few micrometres and more, as in figures 3 (*a*) and (*b*). If the line direction is away from $\langle 110\rangle$, several faults of only a small width form along a single dislocation. This is shown in figures 3 (*c*)–(*f*) for a partly dissociated dislocation having a $\frac{1}{2}[1\bar{1}1]$ Burgers vector and a $[\bar{3}31]$ line direction after an *in-situ* annealing experiment on specimen S. The fault sizes are about 300 mm × 600 nm. The contrast of the non-dissociated parts of the dislocation line disappears using the imaging vectors $(2\bar{1}\bar{3})$ and $(\bar{1}01)$. The enlargement of two faults in figure 3 (*c*) shows preferred $\langle 110\rangle$ line orientations of the partial dislocations. It is consistent with figures 3 (*c*)–(*f*) that partial dislocations with a Burgers vector parallel to [001] moved away from the original $\frac{1}{2}\langle 111\rangle$ dislocation. Their motion on the (001) plane is only possible by climb. Faults on $\frac{1}{2}\langle 111\rangle$ dislocations with line directions different from $\langle 110\rangle$ were formed in central regions as well as near the surfaces of the TEM foils. Thus, an influence of surface effects seems rather unlikely.

Although the average separations of partials bordering the faults depend on the type of the *in-situ* experiment, the individual values scatter markedly. Also, within a single specimen, $\frac{1}{2}\langle 111\rangle$ dislocations do not have to dissociate inevitably at elevated temperatures. After the *in-situ* experiments, all microspecimens contain dissociated and non-dissociated $\frac{1}{2}\langle 111\rangle$ dislocations. The spontaneous and discontinuous formation of the faults only if $\frac{1}{2}\langle 111\rangle$ dislocations are present and the huge separation of the partial dislocations after *in-situ* straining hint at a dissociation reaction of these dislocations including glide of at least one bordering partial dislocation due to the external stress component acting on the (001) planes. On the other hand, figures 2 and 3 (*c*)–(*f*) show a motion of a partial dislocation on (001) planes that is only possible by climb. Thus, both glide and climb processes seem to be involved in the formation of the faults on (001) planes.

4.2. *Transmission electron microscopy characterization of the faults*

The contrast behaviour of the observed planar faults has been analysed by conventional methods of diffraction contrast. Figure 4 shows bright- and dark-field images taken of faults in specimen W. As the TEM foil surface is almost parallel to (010), the faults on (001) planes lie 'edge on' for the direction of the electron beam in figure 4 (*a*). Tilting the specimen around the [100] axis yields the typical fringe contrasts of the interfaces illustrated in figures 4 (*b*) and (*c*). The fringes are invisible with the imaging vectors (200) and $(\bar{1}\bar{1}0)$ in figures 4 (*d*) and (*e*). Hence, $\mathbf{R}_F$ is parallel to [001] and is of the type $\pm(1/m)[001]$, $m = 2$, 3 or 6. Furthermore, the two partial dislocations are extinguished at an (200) imaging vector in figure 4 (*e*) and show a strong residual contrast at $(\bar{1}\bar{1}0)$ in figure 4 (*d*). Thus, the respective Burgers vectors should be parallel to [001]. The contrast behaviour of the fringe patterns has been used to identify the character of the interfaces. The bright- and dark-field images in figures 4 (*b*) and (*c*) respectively have been taken with the imaging vector $(\bar{2}\bar{1}\bar{3})$. The fringes are visible for these fundamental reflections and run parallel to the closest foil surfaces each. In the bright-field image (figure 4 (*b*)), the fringe pattern is symmetrical

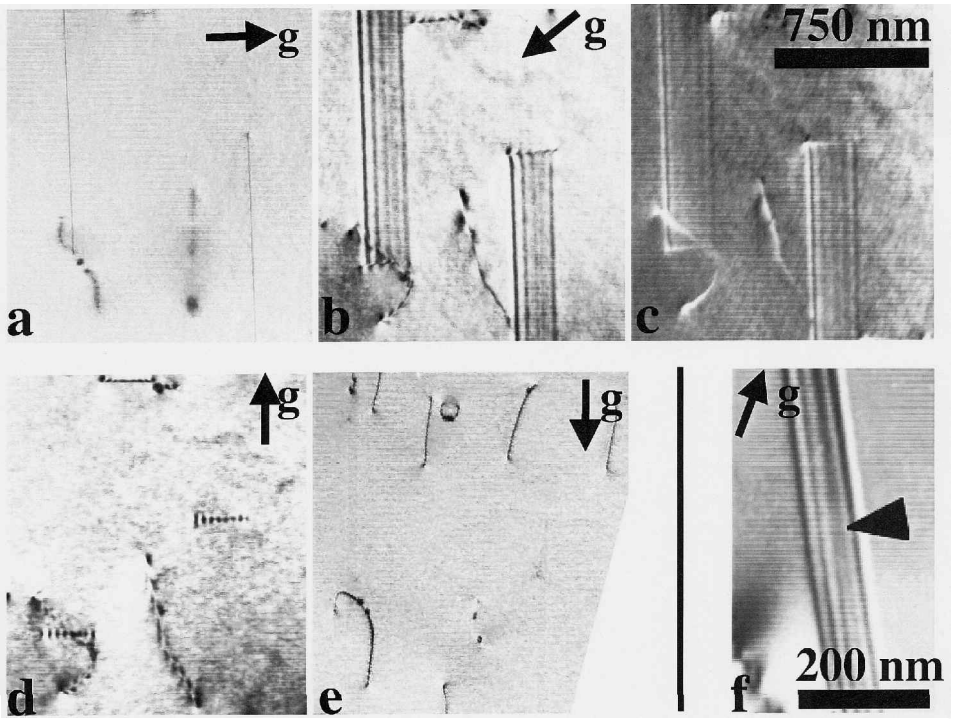

Figure 4. Contrast behaviour of planar faults in specimen W under different imaging conditions: (*a*) $\mathbf{g} = (002)$ and a BD of approximately [010] (equal to foil normal); (*b*) $\mathbf{g} = (\bar{2}\bar{1}3)$ and a BD of approximately $[03\bar{1}]$; (*c*) dark-field image using the same imaging conditions as in (*b*); (*d*) $\mathbf{g} = (200)$ and a BD of approximately $[03\bar{1}]$; (*e*) $\mathbf{g} = (\bar{1}\bar{1}0)$ and a BD of approximately $[\bar{1}10]$; (*f*) uncorrected dark field image, $\mathbf{g} = (\bar{1}0\bar{1})$ and a BD of approximately 12° away from [010]. With increasing thickness, new fringes are created at the centre of the foil.

with respect to the foil centre but asymmetrical in the dark field image (figure 4(*c*)). This pattern is in agreement with that produced by simple stacking faults (Art *et al.* 1963, Gevers *et al.* 1963, Amelinckx *et al.* 1978), that is $\mathbf{R}_F$ can only be $\pm\frac{1}{2}[001]$ or $\pm\frac{1}{6}[001]$. In both the bright- and the dark-field images in figure 4, the left edge fringes have the same contrasts and hence mark the top of the TEM foil. Since the outer fringes are bright in the bright-field image in figure 4(*b*), $\mathbf{R}_F$ is negative for the imaging vector $(\bar{2}\bar{1}3)$ used, that is $\mathbf{R}_F = -\frac{1}{2}[001]$ or $\mathbf{R}_F = -\frac{1}{6}[001]$, which defines the defects as intrinsic stacking faults. Figure 4(*f*) shows a detail of another fault running through a region of changing foil thickness in specimen W. With increasing thickness of the TEM foil a new fringe is created at the centre of the foil. This is again consistent with the fringe contrast of stacking faults (Amelinckx *et al.* 1978).

The determination of the absolute value of the fault vector $\mathbf{R}_F$ is demonstrated in figure 5 on a stacking fault in specimen Q, using the invisibility of the fringe contrast according to equation (4). Therefore, different absolute values of imaging vectors $\mathbf{g}$ of reflecting planes which do not belong to the $\langle 001 \rangle$ zone axis were used to realize different integers of $\mathbf{g} \cdot \mathbf{R}_F$. Values of $\mathbf{g} \cdot \mathbf{R}_F$ are listed in table 2 for all possible $\mathbf{R}_F$ and the applied types of $\mathbf{g}$ vector. The last column presents the visibility of the fringes in figure 5. The results are consistent with fault vectors $\pm\frac{1}{2}[001]$ and $\pm\frac{1}{6}[001]$. Using

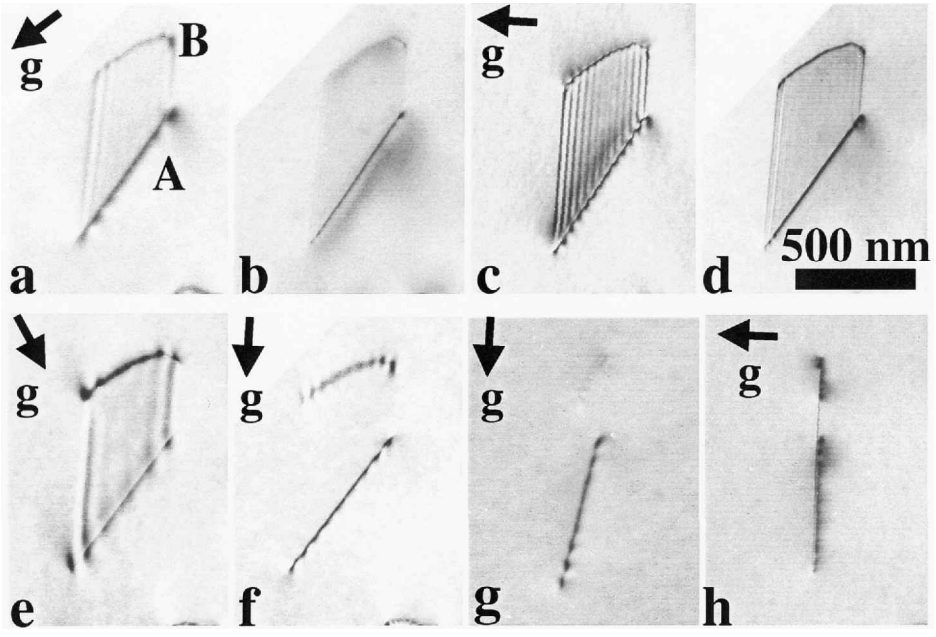

Figure 5. Contrast behaviour of a planar fault and its bordering partial dislocations A and B in specimen Q under different imaging conditions: (a) $\mathbf{g} = (213)$ and a BD of approximately $[03\bar{1}]$; (*b*) $\mathbf{g} = 2 \times (213)$ and a BD of approximately $[03\bar{1}]$; (*c*) $\mathbf{g} = (013)$ and a BD of approximately $[03\bar{1}]$; (*d*) $\mathbf{g} = 3 \times (013)$ and a BD of approximately $[03\bar{1}]$; (*e*) $\mathbf{g} = (2\bar{1}3)$ and a BD of approximately $[03\bar{1}]$; (*f*) $\mathbf{g} = (200)$ and a BD of approximately $[03\bar{1}]$; (*g*) $\mathbf{g} = (200)$ and a BD of approximately [010]; (*h*) $\mathbf{g} = (008)$ and a BD of approximately [010].

fundamental reflections, a distinction is not possible between both, as $\mathbf{g}\cdot\mathbf{R}_F$ for $\mathbf{R}_F = \pm\frac{1}{2}[001]$ will always be three times that for $\mathbf{R}_F = \pm\frac{1}{6}[001]$. The very weak residual contrast in figure 5(*b*) may arise from the fact that $\mathbf{g}\cdot\mathbf{R}_F$ is not exactly an integer value. $\mathbf{R}_F = \pm\frac{1}{3}[001]$ has to be ruled out as the visibility of the fault fringes in figures 5(*a*) and 5(*c*)–(*e*) is not consistent with the respective values of ±1 and ±3 for $\mathbf{g}\cdot\mathbf{R}_F$, in agreement with the fact that the fringes are characteristic of stacking faults but not of antiphase boundaries.

Finally, the Burgers vectors of the partial dislocations bordering the faults were analysed on the basis of figures 5 and 6, where the dislocations are labelled A and B

Table 2. Values of $\mathbf{g}\cdot\mathbf{R}_F$ for different types of imaging vectors $\mathbf{g}$ and fault vectors $\mathbf{R}_F$ corresponding to figure 5.

	$\mathbf{g}\cdot\mathbf{R}_F$ for the following $\mathbf{R}_F$			
$\mathbf{g}$	$\frac{1}{2}[001]$	$\frac{1}{3}[001]$	$\frac{1}{6}[001]$	Visibility of fringes
{213}	$\frac{3}{2}$	1	$\frac{1}{2}$	Visible
$2 \times \{213\}$	3	2	1	Almost invisible
{013}	$\frac{3}{2}$	1	$\frac{1}{2}$	Visible
$3 \times \{013\}$	$\frac{9}{2}$	3	$\frac{3}{2}$	Visible
{200}	0	0	0	Invisible

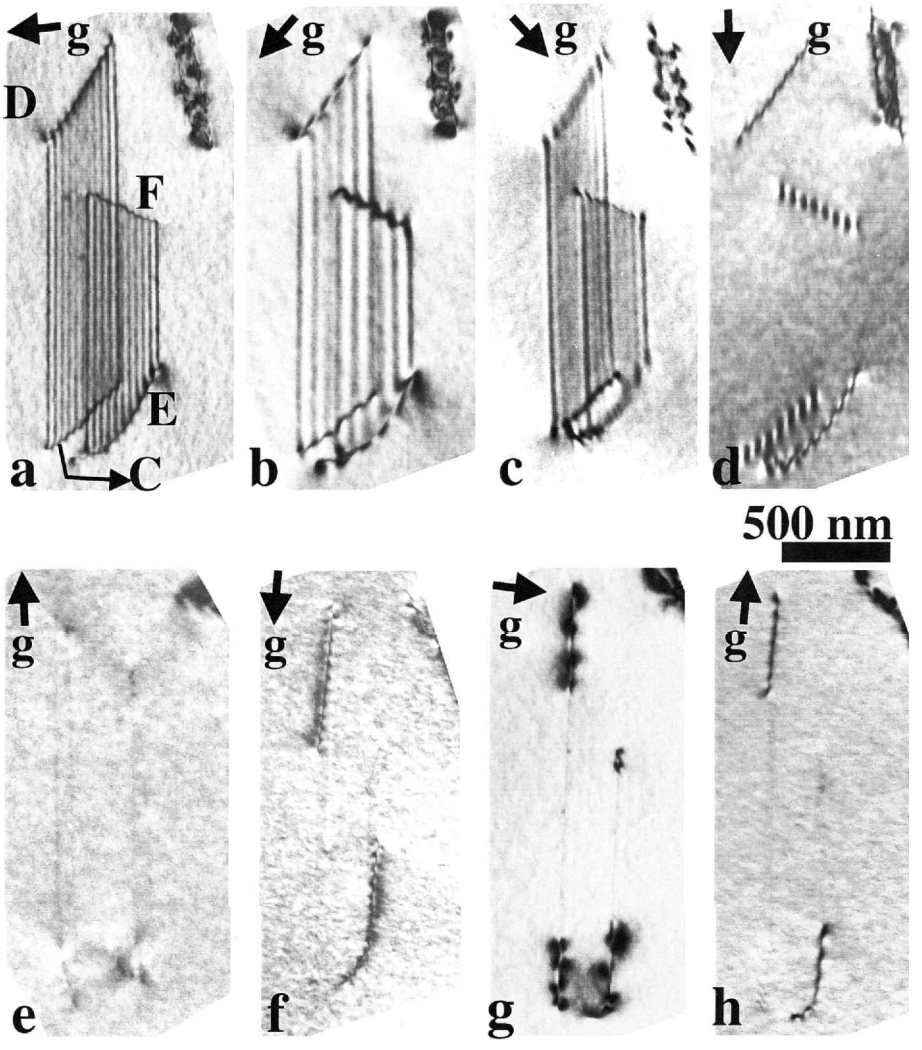

Figure 6. Contrast behaviour of partial dislocations labelled C to F in specimen T for different imaging conditions: (*a*) $\mathbf{g} = (013)$ and a BD of approximately $[03\bar{1}]$; (*b*) $\mathbf{g} = (213)$ and a BD of approximately $[03\bar{1}]$; (*c*) $\mathbf{g} = (2\bar{1}\bar{3})$ and a BD of approximately $[03\bar{1}]$; (*d*) $\mathbf{g} = (200)$ and a BD of approximately $[03\bar{1}]$; (*e*) $\mathbf{g} = (\bar{1}10)$ and a BD of approximately [110]; (*f*) $\mathbf{g} = (110)$ and a BD of approximately $[\bar{1}10]$; (*g*) $\mathbf{g} = (00\bar{2})$ and a BD of approximately [010]; (*h*) $\mathbf{g} = (\bar{2}00)$ and a BD of approximately [010].

as well as C to F. The six dislocations can be divided into two groups with similar extinction behaviour inside each group. Their visibility is listed in table 3 together with the $\mathbf{b}\cdot\mathbf{g}$ values of the imaging vectors used for dislocations with Burgers vectors of $\frac{1}{2}\langle 001\rangle$, $\frac{1}{2}\langle 110\rangle$ and $\frac{1}{6}\langle 331\rangle$. Figures 5 and 6 and table 3 clearly show that the Burgers vectors of the two partial dislocations surrounding a single fault are of different types.

Both partials bordering a fault are visible for all {213} and {013} imaging vectors, which is inconsistent with Burgers vectors parallel to any $\langle 331\rangle$ direction. The Burgers vectors of the partials B, C and F are clearly identified as being parallel

Table 3. $\mathbf{g}\cdot\mathbf{b}$ values of several Burgers vectors $\mathbf{b}$ and imaging vectors $\mathbf{g}$ used in figures 5 and 6 as well as visibility (V), partly in residual contrast, and invisibility (I) of the partial dislocations.

	$\mathbf{g}\cdot\mathbf{b}$ for the following $\mathbf{g}$							
$\mathbf{b}$	(213)	$(2\bar{1}\bar{3})$	(013)	(200) [031]	(200) [010]	(002) (or (008))	$(\bar{1}10)$	(110)
$\frac{1}{2}[001]$	$\frac{3}{2}$	$-\frac{3}{2}$	$\frac{3}{2}$	0	0	1	0	0
$\frac{1}{2}[110]$	$\frac{3}{2}$	$\frac{1}{2}$	$\frac{1}{2}$	1	1	0	0	1
$\frac{1}{2}[\bar{1}10]$	$-\frac{1}{2}$	$-\frac{3}{2}$	$\frac{1}{2}$	-1	-1	0	1	0
$\frac{1}{6}[331]$	2	0	1	1	1	$\frac{1}{3}$	0	1
$\frac{1}{6}[3\bar{3}1]$	1	1	0	1	1	$\frac{1}{3}$	-1	0
Dislocations A, D, E	V	V	V	V	V	V	I	V
Dislocations B, C, F	V	V	V	V	I	V	I	I

to $\langle 001\rangle$ since these dislocations are extinguished for the two $\{110\}$ $\mathbf{g}$ vectors. There is a strange situation for the (200) $\mathbf{g}$ vector. While the same dislocations are invisible for this $\mathbf{g}$ vector taken at the [010] pole in figures 5(*g*) and 6(*h*), they show residual contrasts with the same $\mathbf{g}$ vector taken near the $[03\bar{1}]$ pole, a weak contrast in figure 5(*f*) but a strong contrast in figure 6(*d*). At present, this controversy cannot be explained. The invisibility of dislocations D and E at the $(\bar{1}10)$ reflection in figure 6(*e*) points at a Burgers vector parallel to [110], which, however, is not consistent with the visibility at the (002) and (008) reflections in figure 6(*g*) and of dislocation A in figure 5(*h*). Although the identification of the Burgers vectors of the partial dislocations is not unambiguous, it is argued in §5.1 that they are $\frac{1}{2}\langle 001\rangle$ and $\frac{1}{2}\langle 110\rangle$. Tilting to other poles in order to obtain further $\mathbf{g}$ vectors was not possible because of the limited tilting range of the goniometer stage. The discrepancies should be solved by image simulation, which will be a topic of further research.

§5. Discussion

5.1. *Dissociation of dislocations with* $\frac{1}{2}\langle 111\rangle$ *Burgers vectors*

The most important observations of the present *in-situ* annealing and straining experiments are the following. Planar faults form on (001) planes in $MoSi_2$ at temperatures between 440 and 1000°C. Dislocations with $\frac{1}{2}\langle 111\rangle$ Burgers vectors are involved in this process. The crystals contain these dislocations owing to a predeformation or they are generated by straining during the *in-situ* experiments. The fault vector is parallel to [001], either $-\frac{1}{6}[001]$ or $-\frac{1}{2}[001]$. If the faults emerge through the specimen surface, the bordering partial dislocations have different Burgers vectors. One of them is clearly identified as being parallel to [001], and the other may be parallel to $\langle 110\rangle$. Burgers vectors parallel to $\langle 331\rangle$ are not consistent with the observed contrast behaviour. All the observations can best be explained by a formation of the planar faults by a dissociation of the dislocations with $\frac{1}{2}\langle 111\rangle$ Burgers vectors according to

$$\tfrac{1}{2}[111](1\bar{1}0) \rightarrow \tfrac{1}{2}[001](1\bar{1}0) + \tfrac{1}{2}[110](001). \qquad (5)$$

Reaction (5) leads to faults with a fault vector equal to the absolute value of the Burgers vector of the Frank type partial, that is $\mathbf{R}_F = -\frac{1}{2}[001]$, which is consistent with the results of the presented contrast analysis of the faults. The faults can be created either by climb of the Frank-type dislocation with a $\frac{1}{2}[001]$ Burgers vector or by glide of the partial dislocation with the $\frac{1}{2}[110]$ Burgers vector, both on the (001) plane. The indices in parentheses mark the slip planes of the respective dislocations. Their $\langle 110 \rangle$ intersection line is the preferred orientation of the initial dislocation for dissociation. The (001) plane is not established as a slip plane in $MoSi_2$ but in WSi_2 dislocations with $\langle 100 \rangle$ Burgers vectors move on this plane (Ito *et al.* 1999b). The stacking sequence of the (001) planes resulting from equation (5) is illustrated in figure 7. The fault vector $\mathbf{R}_F = -\frac{1}{2}[001]$ corresponds to a removal of three (001) layers (two Si layers and one Mo layer), without a loss of stoichiometry. The wide separation of the partial dislocations indicates a low stacking-fault energy. Unfortunately, all published data on fault energies concern dislocation dissociations on {013} and {110} planes (Sadananda *et al.* 1991, Evans *et al.* 1993a, b, Ito *et al.* 1995, 1999a, Waghmare *et al.* 1999, Mitchell *et al.* 2001). No data exist for faults with $\mathbf{R}_F = -\frac{1}{2}[001]$. Reaction (5) is energetically neutral since the Burgers vectors of the partials are perpendicular to each other (Hirth and Lothe 1982). For the $\langle 110 \rangle$ orientation, the neutrality is also obtained in a numerical calculation based on elastic anisotropy.

5.2. *Mechanisms of fault formation*

The possibilities of forming the faults by both glide and climb is consistent with the experimental observations. On the one hand, formation always occurred as a

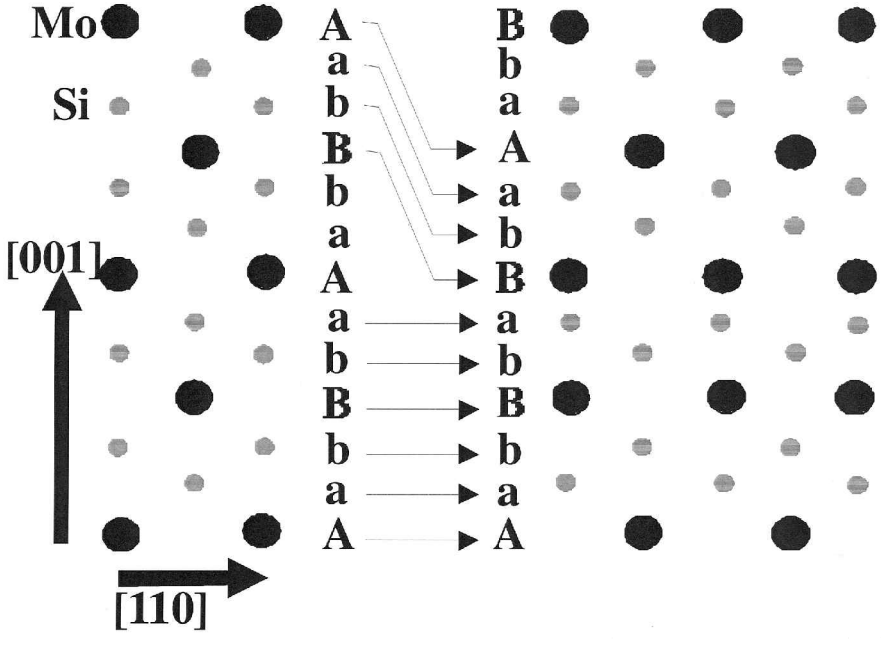

Figure 7. Disorder in the (001) stacking sequence produced by glide of a partial dislocation with a Burgers vector of $\frac{1}{2}[110]$ or climb of a partial dislocation with a Burgers vector of $\frac{1}{2}[001]$.

spontaneous process where later changes in fault sizes have never been observed. The individual sizes of the faults scatter considerably but the average size depends on the type of *in-situ* experiment. Also, in all specimens investigated only some of the $\frac{1}{2}\langle 111\rangle$ dislocations dissociated. These findings point to a discontinuous formation. In accordance with equation (5), $\frac{1}{2}\langle 111\rangle$ dislocations with a line direction near the $\langle 110\rangle$ intersection line between the slip plane of the original dislocation and the fault plane dissociate along their whole line length within a TEM foil, while those dislocations away from a $\langle 110\rangle$ direction only form dissociated segments. These observations suggest that glide of the $\frac{1}{2}\langle 110\rangle$ partial dislocations is essential for the creation of the large faults as in figures 3(*a*) and (*b*), 4 and 5. On the other hand, in annealing experiments, Frank-type partial dislocations had moved away from the original $\frac{1}{2}\langle 111\rangle$ dislocation, dragging several faults of smaller size behind, as shown in figures 3(*c*)–(*f*). This is consistent with a climb process only. The partial dislocations again prefer $\langle 110\rangle$ orientations. Possibly, climb generally initiates the dissociation process. This climb motion requires the diffusion of Mo and Si atoms in the ratio of 1 to 2 or of the respective vacancies. As the diffusion of Mo is expected to be considerably lower than that of Si (Matsuda *et al.* 1998, Ito *et al.* 1999a, Sadananda *et al.* 1999), the mobility of Mo atoms or vacancies should control the climb velocity. After nucleation, the faults may extend by glide if the $\frac{1}{2}\langle 110\rangle$ partial dislocations are long enough and experience a respective shear stress. Such a shear stress is present during *in-situ* straining and leads there to the very wide faults, but it is not present in the annealing experiments.

The formation of the stacking faults may be influenced by the special conditions during the *in-situ* experiments. During observation in the high-voltage electron microscope with an accelerating voltage of 1 MeV, the specimens are exposed to high-energy electron irradiation which can produce vacancies on Si lattice sites (Matsuda *et al.* 1998, Ito *et al.* 1999a). However, the vacancies generated by 1 MeV electron irradiation become mobile at temperatures between 240 and 300 K, forming secondary defects which anneal out around 500 K (Matsuda *et al.* 1998, Ito *et al.* 1999a). All *in-situ* annealing and straining experiments were carried out above 500 K. Thus, the vacancies generated by electron bombardment during the *in-situ* experiments should easily anneal out so that faults should not form by condensation of irradiation-induced vacancies. Furthermore, planar faults on (001) planes in $MoSi_2$ have never been observed to form during the TEM analysis at elevated temperatures or room temperature in precipitation-free and dislocation-free crystal areas. Therefore, radiation damage may play a role in the nucleation of the faults at dislocations but it is not the only origin of these defects.

The initial climb processes may result from the condensation of either thermal or structural vacancies. The latter should not be present in high concentrations (Matsuda *et al.* 1998). Also, heating the specimens to 1200°C in the high-voltage electron microscope did not lead to the generation of faults in precipitation-free and dislocation-free crystal areas. Thus, the condensation of thermal vacancies in an otherwise defect-free $MoSi_2$ single crystal cannot be regarded as the only origin of the faults. The condensation of vacancies would lead to Frank-type loops, which should be of medium size (10–50 nm diameter) or small size (less than 10 nm diameter) instead of the observed wide faults, and they should grow in a slow continuous way. Inhomogeneous nucleation of Frank loops is possible on dislocations and Mo_5Si_3 precipitates, but the faults were never detected on defects other than dislocations with $\frac{1}{2}\langle 111\rangle$ Burgers vectors, for example $\langle 100\rangle$ dislocations generated during

compression tests in specimens O, P and X, or on Mo_5Si_3 precipitates, which often occur in CZ crystals.

Surface effects of the TEM foils may influence the formation of the faults in two ways. It is well known that $MoSi_2$ loses Si at high temperatures in vacuum. The loss of Si leads to Si vacancies which may induce the dislocations to climb. However, all mechanisms based on the diffusion of Si vancancies alone are not consistent with the fault vector of $-\frac{1}{2}[001]$ suggested above which corresponds to two Si missing layers and one Mo missing layer. The proximity of the crystal surfaces gives rise to image forces on the dislocations. These forces may support the dissociation of the dislocations with $\frac{1}{2}\langle 111\rangle$ Burgers vectors. Most specimens had a [010] foil normal so that the faults on (001) planes are arranged edge on. Then, the partial dislocations with $\frac{1}{2}\langle 110\rangle$ Burgers vectors may be induced to move out of the foil, dragging the faults. This may explain why the faults do not form during bulk deformation with glide of dislocations with $\frac{1}{2}\langle 111\rangle$ Burgers vectors.

5.3. *Comparison with previous literature*

A detailed analysis of planar faults in $MoSi_2$ has already been presented by Kad *et al.* 1995, who reinterpreted the results on faults on (001) planes of earlier investigations by Umakoshi *et al.* (1989, 1990). Regarding the TEM results, the interpretation of Kad *et al.* (1995) may also be applied to the results of Kimura *et al.* (1990) and Hirano *et al.* (1991). It is considered that the faults may already exist prior to the applied deformation and that they are thermally stable intrinsic condensation faults on (001) planes in $MoSi_2$ with $\mathbf{R}_F = -\frac{1}{6}[001]$. A loss of a single Si layer at high temperatures during crystal growth, which is caused by a deviation from stoichiometry, is thought to be responsible for the fault formation. Such intrinsic faults should be bordered by Frank type partial dislocations. Unfortunately, the Burgers vector analysis by Kad *et al.* (1995) is insufficient as it treats one partial dislocation only. As shown in the present study, the Burgers vectors of the bordering partials are different so that both partials have to be analysed. Also, the faults extend over at least a few micrometres, which is inconsistent with the homogeneous nucleation of a great number of Frank loops of small size at a loss of Si.

Contrary to Kad *et al.* (1995), Ito *et al.* (1997) and Inui *et al.* (2001) revealed a fault vector $\mathbf{R}_F = \frac{1}{3}[001]$ in $MoSi_2$ and WSi_2, both of the $C11_b$ structure, from experimental and calculated high-resolution TEM images. Here, again extended faults but only one partial dislocation of Frank type are analysed. Although the faults are described by a removal of two adjacent Si layers, that is they are of intrinsic nature, the contrast behaviour of the fringe pattern shown for faults in WSi_2 is consistent with a positive $\mathbf{R}_F$, that is with extrinsic faults. The distinct fringe patterns for {013} imaging vectors are explained by strong deviations from an exact fault vector $\mathbf{R}_F = \frac{1}{3}[001]$ for faults in both $MoSi_2$ and WSi_2, which exceed the limit of deviations from the exact $\mathbf{g}\cdot\mathbf{R}_F$ of 0.02 for effective extinctions as stated by Hirsch *et al.* (1965). However, $\mathbf{R}_F$ of the order of $\frac{1}{3}[001]$ is correlated to antiphase boundary-like fringe contrasts of the faulted planes, while Ito *et al.* (1997) and Inui *et al.* (2001) present stacking fault-like fringe contrasts of faults on (001) planes in $MoSi_2$ and WSi_2. In the present work, $\mathbf{R}_F = \frac{1}{3}[001]$ is clearly rejected because of the visibility of the faults in figures 5(*a*) and 5(*c*)–(*e*) with $\mathbf{g}$ vectors of {123} and {013} type.

According to the literature, the loss of Si during crystal growth may cause the formation of different defects, Mo_5Si_3 precipitates in crystals grown by the Czochralski method (for example Boldt *et al.* (1997)) and planar faults on (001)

planes in such made by the FZ technique (Kad *et al.* 1995). In the present study, the CZ crystals also contained Mo_5Si_3 precipitates. However, the formation of planar faults in the FZ crystals clearly depended on the presence of dislocations with $\frac{1}{2}\langle 111\rangle$ Burgers vectors. However, the present TEM analysis is inconsistent with the previous dissociation reactions (2) and (3). Equation (2) is accompanied by a complex stacking fault on (001) planes and requires three partial dislocations. Equation (3) suggests one partial dislocation having a Burgers vector parallel to a $\langle 331\rangle$ direction and an antiphase-boundary-like contrast of the faulted plane. Such defects have been observed by Mitchell and Maloy (1993) and Maloy *et al.* (1995) as a product of climb during compression with corresponding fault widths of 5–50 nm. The faults observed in this study are mostly much wider and of different fringe characteristics.

5.4. *Correlation between the fault formation and the deformation mechanism*

The planar faults are formed in annealing experiments at temperatures above 550°C and in straining experiments above 440°C. This temperature range coincides with the onset temperature of 500°C of the flow stress anomaly of the $\langle 111\rangle\{110\}$ slip system observed during macroscopic deformation of the same crystals by Guder *et al.* (1999) and Guder (2000). The flow stress anomaly of the $\langle 111\rangle\{110\}$ slip system was observed before by other researchers (for example Ito *et al.* (1995)). Observations of the dislocation dynamics during *in-situ* straining experiments and measurements of the strain-rate sensitivity indicate the occurrence of dynamic strain ageing in the anomaly range of the $\langle 111\rangle\{110\}$ slip system (Messerschmidt *et al.* 1998, 1999, 2001a, b, Guder *et al.* 1999, Guder 2000). In $MoSi_2$, the flow stress anomaly is connected with a transition of the dominating character of mostly straight 60° dislocations with $\frac{1}{2}\langle 111\rangle$ Burgers vectors from an orientation along $\langle 111\rangle$ at and below 500°C (e.g. in specimens H, I, R, S, U and V) to dislocations oriented along $\langle 110\rangle$ at higher temperatures (e.g. in specimens J, K to N, Q, T and W) (Guder 2000, Messerschmidt *et al.* 2001a, b). The occurrence of straight oriented dislocations cannot be explained by a general diffusion model of dynamic strain ageing as done originally by Messerschmidt *et al.* (1998, 1999) but should be connected with a special core configuration. Therefore, a climb dissociation of the dislocations with $\frac{1}{2}\langle 111\rangle$ Burgers vectors was later proposed (Messerschmidt *et al.* 2001b):

$$\tfrac{1}{2}[111](1\bar{1}0) \rightarrow \tfrac{1}{6}[331](1\bar{1}0) + \tfrac{1}{6}[3\bar{3}1](\bar{1}16) + \tfrac{1}{6}[\bar{3}31](1\bar{1}6). \qquad (6)$$

Again, the $\langle 110\rangle$ direction is the intersection line of the three slip planes involved. For this orientation, the latter two partials are of pure edge character, which results in a maximum resistance for the conservative climb, which is necessary to move the whole dislocation on the $(1\bar{1}0)$ plane. Apparently, the $\frac{1}{2}\langle 111\rangle$ dislocation along $\langle 110\rangle$ is particularly unstable and can dissociate according to either equation (5) or equation (6), possibly depending on the local stress state. Both dissociations may be initiated by climb, by usual climb under a small supersaturation in the case of equation (5) or by conservative climb between the two edge partials for equation (6). Climb dissociation of superdislocations was first suggested by Saka and Zhu (1985, 1989) as the origin of the flow stress anomaly.

There are similarities in the deformation behaviour of the $\{110\}\langle 111\rangle$ slip system in $MoSi_2$ and WSi_2 as stated by Ito *et al.* (1999b). There again, the $\frac{1}{2}\langle 111\rangle$ dislocations show a strong tendency to align along the $\langle 110\rangle$ direction on $\{110\}$ planes for deformation temperatures above 1000°C. During the high-temperature deformation, a great number of stacking faults are created. This emphasizes the connection

between the deformation parameters and dislocation dissociations leading to stacking faults. Further investigations are necessary to elucidate possible similarities of the mechanisms of the formation of stacking faults and the temperature-dependent flow stress of $MoSi_2$, WSi_2 and solid solutions of both.

§6. Conclusions

(1) Planar faults on (001) planes are formed in $MoSi_2$ during *in-situ* annealing and straining experiments in a high-voltage transmission electron microscope between 440 and 1000°C if dislocations with $\frac{1}{2}\langle 111\rangle$ Burgers vectors are present, either from a pre-deformation or generated during *in-situ* straining.

(2) The density and size of the defects depend on the orientation of the initial dislocations. The $\langle 110\rangle$ orientation is a preferred orientation for the formation of the faults.

(3) The faults are intrinsic stacking faults, most probably having a fault vector of $-\frac{1}{2}[001]$ corresponding to a loss of two Si planes and one Mo plane without violating the stoichiometry of the crystals.

(4) The faults are bordered by partial dislocations of different Burgers vectors, which can be explained by a dissociation of the initial dislocations according to $\frac{1}{2}[111] = \frac{1}{2}[001] + \frac{1}{2}[110]$, by climb of the $\frac{1}{2}[001]$ partial and/or by glide of the $\frac{1}{2}[110]$ partial, leading to the large fault widths.

(5) The microprocesses of the fault formation seem to be related to those of the flow stress anomaly.

Acknowledgements

The authors thank S. Maloy, Los Alamos National Laboratory, New Mexico, USA, and M. Yamaguchi, Kyoto University, Japan, for supplying the single crystals and Ch. Dietzsch and W. Greie for technical assistance. Funding of the work by the Volkswagenstiftung is gratefully acknowledged.

References

Amelinckx, S., Gevers, R., and Van Landuyt, J., 1978, *Diffraction and Imaging Techniques in Material Science*, second edition (Amsterdam: North-Holland), p. 107.

Art, A., Gevers, R., and Amelinkcx, S., 1963, *Phys. Stat. sol.*, **3**, 697.

Boettinger, W. J., Perepezko, J. H., and Frankwicz, P. S., 1992, *Mater. Sci. Engng* **A155**, 33.

Boldt, P., Wheatherly, G. C., and Embury, J. D., 1997, *Phil. Mag.* A, **75**, 97.

Evans, D. J., Court, S. A., and Hazzledine, P. M., 1993a, *Phil. Mag. Lett.*, **67**, 331.

Evans, D. J., Court, S. A., Hazzledine, P. M., and Fraser, H. L. 1993b, *High-Temperature Ordered Intermetallic Alloys V*, Materials Research Society Symposium Proceedings, Vol. 288, edited by I. Baker, J. Darolia, J. D. Whitten and M. H. Yoo (Pittsburgh, Pennsylvania: Materials Research Society), pp. 567–572.

Evans, D. J., Scheltens, F. J., Woodhouse, J. B., and Fraser, H. L., 1997, *Phil. Mag.* A, **75**, 17.

Frankwicz, P. S. Perepezko, J. H., and Anton, D. L., 1993, *High-Temperature Ordered Intermetallic Alloys V*, Materials Research Society Symposium Proceedings, Vol. 288, edited by I. Baker, J. Darolia, J. D. Whitten and M. H. Yoo (Pittsburgh, Pennsylvania: Materials Research Society), pp. 159–164.

Gevers, R., Art, A., and Amelinckx, S., 1963, *Phys. Stat sol.*, **3**, 1563.

Guder, S., 2000, PhD Thesis, Martin-Luther-Universität, Halle-Wittenberg, Merseburg.

Guder, S., Bartsch, M., Yamaguchi, M., and Messerschmidt, U., 1999, *Mater. Sci. Engng*, A **261**, 139.

HIRANO, T., NAKAMURA, M., KIMURA, K., and UMAKOSHI, Y., 1991, *Ceram. Engng Sci. Proc.*, **12**, 1619.
HIRSCH, P. B., HOWIE, A., NICHOLSON, R. B., PASHLEY, D. W., and WHELAN, M. J., 1965, *Electron Microscopy of Thin Crystals* (London: Butterworth), p. 165.
HIRTH, J. P., and LOTHE, J., 1982, *Theory of Dislocations* (New York: Wiley).
INUI, H., ITO., K., NAKAMOTO, T., ISHIKAWA, K., and YAMAGUCHI, M., 2001, *Mater. Sci. Engng*, **314**, 31.
ITO, K., INUI, H., SHIRAI, Y., and YAMAGUCHI, M., 1995, *Phil. Mag.* A, **72**, 1075.
ITO, K., MATSUDA, K., SHIRAI, Y., INUI, H., and YAMAGUCHI, M., 1999a, *Mater. Sci. Engng*, **261**, 99.
ITO, K., NAKAMOTO, T., INUI, H., and YAMAGUCHI, M., 1997, *High-Temperature Ordered Intermetallic Alloys VII*, Materials Research Society Symposium Proceedings, Vol. 460, edited by C. C. Koch, C. T. Liu, N. S. Stoloff and A. Wanner (Pittsburgh, Pennsylvania: Materials Research Society), pp. 599–604.
ITO, K., YANO, T., NAKAMOTO, T., INUI H., and YAMAGUCHI, M., 1996, *Intermetallics*, **4**, S119; 1999b, *Acta metall. mater.*, **47**, 937.
KAD, B. K., VECCHIO, K. S., ASARO, R. J., and BEWLAY, B. P., 1995, *Phil. Mag.* A, **72**, 1.
KIMURA, K., NAKAMURA, M., and HIRANO, T., 1990, *J. Mater. Sci.*, **25**, 2487.
MALOY, S. A., MITCHELL, T. E., and HEUER, A. H., 1995, *Acta metall. mater.*, **43**, 657.
MATSUDA, K., SHIRAI, Y., and YAMAGUCHI M., 1998, *Intermetallics*, **6**, 395.
MESSERSCHMIDT, U., and BARTSCH, M., 1994, *Ultramicroscopy*, **56**, 167.
MESSERSCHMIDT, U., BARTSCH, M., GUDER, S., and HÄUßLER, D., 1999, *High-Temperature Ordered Intermetallic Alloys VIII*, Materials Research Society Proceedings, Vol. 552, edited by E. P. George, M. J. Mills and M. Yamaguchi (Pittsburgh, Pennsylvania: Materials Research Society), pp. KK10.9.1–KK10.9.6.
MESSERSCHMIDT, U., BARTSCH, M., GUDER, S., HÄUßLER, D., HAUSHÄLTER, R., and YAMAGUCHI, M., 1998, *Intermetallics*, **6**, 729.
MESSERSCHMIDT, U., GUDER, S., HÄUSSLER, D., and BARTSCH, M., 2001a, CD-ROM special issue of *J. Mater. Processing Technol.*, **117**, 3.
MESSERSCHMIDT, U., GUDER, S., JUNKER, L., BARTSCH, M., and YAMAGUCHI, M., 2001b, *Mater. Sci. Engng*, **A319–A321**, 342.
MITCHELL, T. E., BAKES, M. I., CHEN, S. P., HIRTH, J. P., and HOAGLAND, R. G., 2001, *Phil. Mag.* A, **81**, 1079.
MITCHELL, T. E., and MALOY, S. A., 1993, *Critical Issues in the Development of High Temperature Structural Materials*, edited by N. S. Stoloff, D. J. Duquette and A. F. Giamei (Warrendale, Pennsylvania: Mineral, Metals and Materials Society), pp. 279–290.
SADANANDA, K., FENG, C. R., MITRA, R., and DEEVI, S. C., 1999, *Mater. Sci. Engng*, **A261**, 223.
SADANANDA, K., JONES, H., and FENG, J., 1991, *Ceram. Eng. Sci. Proc.*, **12**, 1671.
SAKA, H., and ZHU, Y. M., 1985, *Phil. Mag.* A, **51**, 629; 1989, *Mater. Sci. Engng*, **A113**, 305.
UMAKOSHI, Y., SAKAGAMI, T., HIRANO, T., and YAMANE, T., 1990, *Acta metall. mater.*, **38**, 909.
UMAKOSHI, Y., SAKAGAMI, T., and YAMANE, T., 1989, *Phil. Mag. Lett.*, **59**, 159.
WAGHMARE, U. V., BULATOV, V., KAXIRAS, E., and DUESBERY, M. S., 1999, *Phil. Mag.* A, **79**, 655.